Assignment of the Fine Structure in the Optical Absorption Spectra of Soluble Single-Walled Carbon Nanotubes

Yongfu Lian,[†] Yutaka Maeda,[†] Takatsugu Wakahara,[†] Takeshi Akasaka,*[,†] Said Kazaoui,[‡] Nobutsugu Minami,[‡] Nami Choi,[‡] and Hiroshi Tokumoto[‡]

Center for Tsukuba Advanced Research Alliance (TARA Center), University of Tsukuba, Tsukuba, Ibaraki 305-8577, Japan, and National Institute of Advanced Industrial Science and Technology, Tsukuba, Ibaraki 305-8562, Japan

Received: April 24, 2003; In Final Form: July 14, 2003

Raw electric-arc-produced single-walled carbon nanotubes (SWNTs) were dispersed in organic solvents via a three-step wet chemistry procedure. The soluble sample was purified by continuous dispersion−centrifugation cycles and well-separated SWNTs with high purity were successfully obtained, which enable us to test the separated tube properties and make comparisons with theoretical predictions. Optical absorption experiments on such prepared samples yield fine structures. A series of optical absorptions including some unobserved in previous works are identified. On the basis of the electronic band theory, all the spectral features are systematically assigned to the electronic transitions between pairs of van Hove singularities of semiconducting and/or metallic SWNTs. Detailed analysis of the optical absorption and Raman scattering data reveals that electric-arc-produced SWNTs are preferentially formed with seven discrete diameters and with chirality close to the armchair direction, and a chiral indices (*n*, *m*) assignment was initially made for those SWNTs dispersed in the solution phase.

1. Introduction

Single-walled carbon nanotubes (SWNTs) can be metallic (*met*-) or semiconducting (*sem*-) depending on their diameters and chiralities, which largely decides their electronic and optical properties. On the other hand, optical absorption spectroscopy is a unique tool for characterizing the electronic structure of SWNTs, and hence gives valuable information on their type (*met*- or *sem*-), diameter, and chirality. Kataura et al.[1] first applied this technique to SWNTs and observed three absorption bands, originating from the overlapping van Hove transitions of varying size SWNTs. They also confirmed the inversely proportional relationship between the nanotube diameter and the energy of the absorption features, just as was predicted by theoretical calculation.[2] Through detailed analysis of the fine structure of optical absorptions, Jost et al.[3] suggested that SWNTs close to armchair chirality are preferentially formed in the laser-vaporization process. To date, optical absorption data obtained from SWNT thin films are commonly used to determine the mean diameter and diameter distribution in bulk SWNTs samples,[4] to investigate the effects of chemical and electrochemical doping and functionalization on the electronic states of *sem*- and *met*-SWNTs,[5−7] etc.

Determination of the electronic and atomic structures of SWNTs undoubtedly is very important for the fundamental research and application development of such novel materials. However, few techniques can be used to assign certain chiral indices (*n*, *m*) to a single SWNT. Though resonant Raman scattering and scanning tunneling microscopy/spectroscopy (STM/STS)[8,9] succeed to some extent with thin solid film samples, there is still lack of experimental tools for in-situ structural identification of SWNTs in solution phase. In contrast to thin solid film, SWNTs well dispersed in liquid medium usually show high-energy resolution in optical absorption spectra,[10,11] which makes it possible to accurately determine the interband transition energy between the van Hove singularities (VHSs) of the density of states and hence the atomic structure of SWNTs. Liquid-phase optical absorption spectroscopy can also be used to measure the dissolution/dispersion quality of SWNTs in some solvents/composites, and offers information on the reaction site of SWNTs upon functionalization. It has been evidenced that chemical modification of the nanotube tips has little effects on absorption bands. In contrast, significant modification of the nanotube sidewalls leads to a complete loss of features in solution-phase absorption spectroscopy.[12] Moreover, achieving and manipulating SWNTs individually is a prerequisite for some practical applications such as nanometer-sized electronic devices and biological sensors.[13] Despite some progress toward this target,[14,15] it is still a challenge to obtain individual SWNTs from their large bundles. Chemical functionalization provides a flexible and effective approach to unbundle, to purify, and even to separate SWNTs in the liquid phase and to assemble them into larger structures.[16−18]

In this paper, we describe a procedure based on wet chemistry and dispersion−centrifugation cycles to disperse and purify the electric-arc-produced soot into well-separated SWNTs. The high resolution shown in the optical adsorption spectra of our soluble samples leads us to resolve weak optical features originating from SWNTs. More than twenty optical subpeaks, some of them not observed in previous works, are identified in the ultraviolet and visible ranges. In line with the electronic band theory, all

* Author to whom correspondence should be addressed. Tel & Fax: (81)-298-53-6409. E-mail akasaka@tara.tsukuba.ac.jp.
[†] University of Tsukuba.
[‡] National Institute of Advanced Industrial Science and Technology.

10.1021/jp035118r CCC: $25.00
Published on Web 10/11/2003

the optical features are ascribed to the interband electronic transitions between pairs of VHSs of *sem*- and/or *met*-SWNTs with seven discrete diameters. Information on chirality distribution is also extracted by fitting to the calculated optical absorption functions, and a chiral indices (*n*, *m*) structural assignment is made for these SWNTs dissolved in organic solvent.

2. Experimental Section

A three-step wet chemistry procedure was applied in this work. First, 200 mg of raw CarboLex SWNT product, purchased from Carbon Solutions, Inc., was dispersed in 150 mL of aqueous $K_2S_2O_8$ (0.2 M) ultrasonically. After adding 25 mL of 97% H_2SO_4, the mixture was magnetically stirred for 24 h at 60 °C. With the reaction mixture cooled, a SWNTs deposit appeared. The upper yellow solution was decanted, and the lower black suspension was further dispersed in 200 mL of distilled water. The decanting/dispersion process was recycled till a stable suspension formed (pH ~ 6−7). After filtration with 1 μm PTFE microfilm, a sample quite easily dispersed in water, DMF, and other polar solvents was obtained.

The purpose of the $K_2S_2O_8$ treatment in H_2SO_4 is to oxidize the carbon materials existing in the pristine SWNTs sample to a varying extent and to partly remove amorphous carbon and metal catalysts. Though $K_2S_2O_8$ is a strong oxidative agent in acid medium, it is still a mild chemical to carbon materials, owing to its usual low chemical reaction rate. The good dispersibility in water of a SWNT sample obtained in this way indicates that some hydrophilic groups such as carboxyl and hydroxyl are generated and that SWNTs are unbundled to some extent. Because of their larger surface areas and higher reactivity, amorphous carbons ought to be oxidized to a much larger degree under our experimental conditions than SWNTs and carbon particles. An atomic force microscopy (AFM) image (not shown here) of the oxidized sample shows that following the $K_2S_2O_8$ treatment the well-oxidized amorphous carbons are coating on the surface of SWNTs without obvious damage to the nanotube structure. Thus, $K_2S_2O_8$ oxidation plays roles in modifying, unbundling, and coating SWNTs, which are important for their further functionalization and purification to obtain a high-quality nanotube sample.

Second, the $K_2S_2O_8$-oxidized SWNTs are further oxidized, cut, polished, and purified by successive sonication in the mixtures of H_2SO_4/HNO_3 (3:1) and H_2SO_4/H_2O_2 (4:1). The sample after H_2SO_4/H_2O_2 treatment was completely washed with water to remove any physically absorbed chemicals and heated in a vacuum at 120 °C overnight.

Finally, into a 500 cm^3 round-bottom flask 150 mg of cut-SWNTs, 1.5 g of octadecylamine (ODA), 1.3 g of dicyclohexylcarbodiimide (DCC), and 300 cm^3 of tetrahydrofuran (THF) were charged. The mixture was stirred with a magnetic stirrer and refluxed at the boiling point of THF for 3 days. When cooled to room temperature, the reaction mixture was diluted with 300 cm^3 THF and then was initially centrifuged at 3000 rpm for 24 h. The upper suspension was carefully decanted and monitored by a UV−vis−NIR spectrophotometer. The sludge thus obtained was dispersed in a proper amount of THF by a brief sonication, and then subjected to further centrifugation. The dispersion/centrifugation process was repeated until no obvious absorptions from SWNTs are observed in the decanted suspension. After 10 times of dispersion/centrifugation cycles, about half of the starting material is left as a residue which is not easily dispersed in THF. We refer to the samples thus obtained as Solution 1, 2, 3, ..., and 10, according to the times of dispersion/centrifugation cycles.

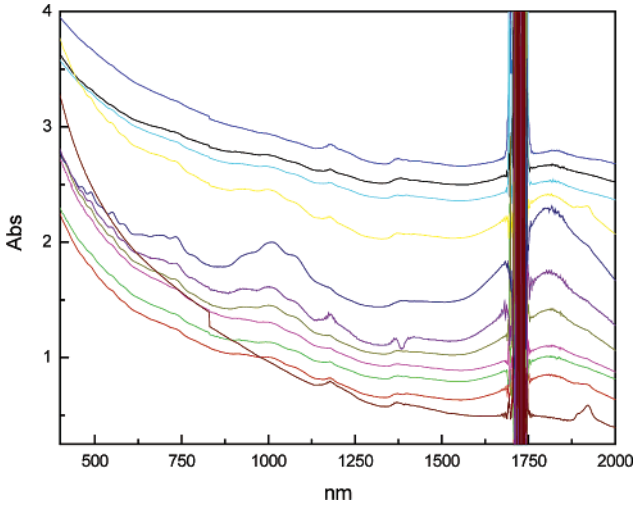

Figure 1. Absorption spectra of the initial suspension and Solutions 1 to 10 (from bottom to top) in the visible and near-infrared ranges. The spectra are offset for clarity, but the intensity scale is identical for all plots.

The reaction between the shortened SWNTs, ODA and DCC could be expressed by the chemical reaction below.

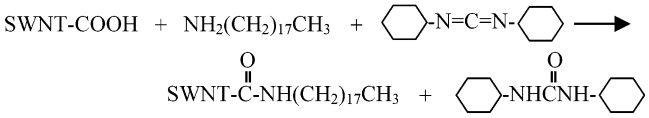

Long alkyl chains are covalently attached to the shortened SWNTs by condensation reaction between the amine group of ODA and the carboxyl group at the ends as well as the wall of SWNTs.[20] DCC plays a role of condensing agent, which combines with water to form *N*,*N*-dicyclohexylurea. The attachment of long alkyl chains leads to the unbundling and solubilization of SWNTs in THF and other organic solvents.

Optical absorption data were measured using a Shimadzu UV-3150 spectrophotometer covering from the near-infrared region to the ultraviolet with a spectral resolution of 2 cm^{-1}. Raman scattering measurements were performed on a Jasco NRS-2100 laser Raman spectrophotometer with an exciting laser of 514.5 nm. The samples were prepared by filtering the fractionated solutions with 0.1 μm PTFE microfilm and subsequently dried for 1 day in a vacuum at 150 °C. Atomic force microscopy (AFM) observations were carried out with Nanoscope III, Digital Instruments, Santa Barbara, CA. Well-dispersed soluble SWNTs were dropped and dried on a freshly cleaved mica surface and observed in the tapping-mode of operation.

3. Results and Discussion

In the optical spectra of electric-arc-produced SWNTs, three characteristic absorption bands are usually observed at approximately 1800, 1000, and 700 nm, respectively, superimposed on a broad background.[1] The first two bands are attributed to electronic transitions between the first and second pairs of VHSs in *sem*-SWNTs, and the last one to the first pair of singularity in *met*-SWNTs. Figure 1 shows the absorption spectra of Solutions 1 to 10 in the visible and near-infrared ranges. To account for the difference in tube concentration, all of the plots were normalized at 1010 nm. It can be seen that the absorption bands mentioned above are observable in our soluble samples prominently or less distinctly. The steplike change of absorption at around 835 nm is an artifact from the spectrophotometer. The shoulders around 1920 and 1180 nm

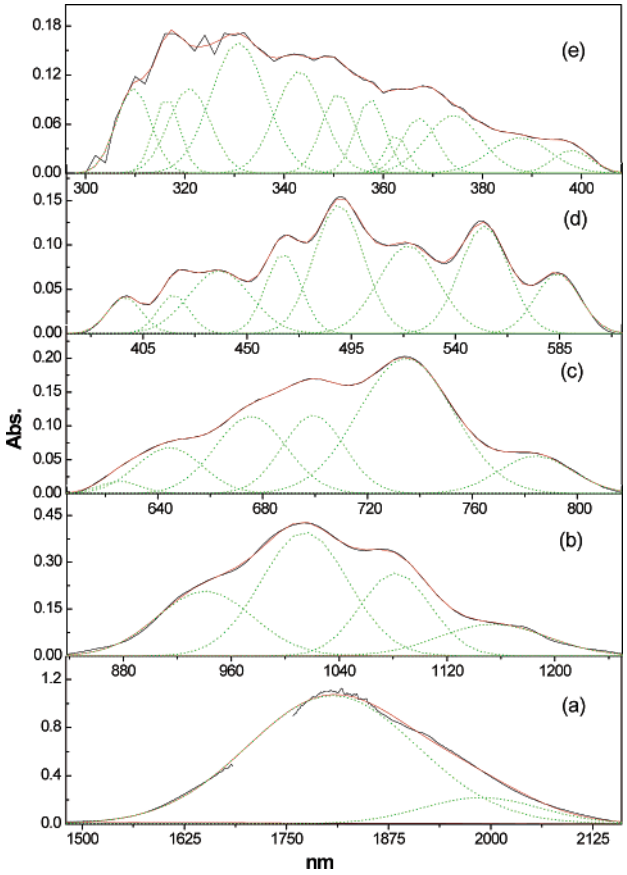

Figure 2. The UV−vis−NIR spectrum of Solution 6 after background correction (the black lines) with Gauss fitting (the green dot and red lines). The break between 1685 and 1760 nm is due to the cutoff of THF absorption.

and the broad absorption bands at 1382 nm are due to the absorbed water in the THF solution. Unfortunately, Chattopadhyay et al.[21] assigned them to the first or second interband transitions of *sem*-SWNTs with varying diameters. It can be seen from Figure 1 that the resolution in optical adsorption spectra improves gradually from Solution 1 to 6, corresponding to gradual decrease of fine functionalized impurities. In contrast, the resolvability of optical adsorption spectra gets lower and lower from Solution 6 to 10, indicating that more impurities and larger bundle of SWNTs transform into the liquid phase. Figure 1 approves the validity of our dispersion/centrifugation cycles in obtaining well-separated SWNTs of high purity. Therefore, optical absorption spectroscopy also offers a convenient and effective method to evaluate the purity and aggregating state of SWNTs. Of interest is to note that Solution 6 displays the most pronounced features among the 10 soluble samples, and detailed study of them will lead to a better understanding of the band structure of the electric-arc-produced SWNTs.

Demonstrated in Figure 2 is the UV−vis−NIR spectrum of Solution 6 in the range of 300−2100 nm after baseline correction. More subpeaks or shoulders are resolved here than in previous optical studies on electric-arc-produced SWNTs.[22,23] These features could be correlated with a series of distinct electronic transitions between the pairs of VHSs of *sem*- and *met*-SWNTs.

According to the electronic band theory,[24] the vertical interband transition energy between the *i*th pair of VHSs in both the valence and the conduction bands of a semiconducting (S) or metallic (M) nanotube ($^{S,M}E_{ii}$) are correlated with the diameter of the SWNT (d_t) by

$$^{S,M}E_{ii} = 2na_{C-C}\gamma_0/d_t$$

where a_{C-C} is the nearest-neighbor carbon−carbon distance (~0.144 nm), γ_0 is the nearest-neighbor carbon−carbon interaction energy (~2.9 eV), and n is an integer. $^{S,M}E_{ii}$ corresponds to the first, second, third, fourth, and fifth interband transition of semiconducting SWNTs when n = 1, 2, 4, 5, and 7, and to the first and second interband transition of metallic SWNTs when n = 3 and 6, respectively. Because of the Coulomb effect,[25] which leads to the absorption feature due to the lowest band-to-band transition shifts to the higher-energy side compared to the transition calculated by a tight-binding model, an energy calibration for the first semiconducting interband transition is made by a factor of 6.0/6.75, on the basis of the measurements of electron energy loss spectroscopy.[26]

The first interband transition of *sem*-SWNTs (Figure 2a) is observed as a broad band over 1490 to 2145 nm with a maximum at 1806 nm. The diameter distribution and mean diameter can be obtained from the width and absorption maximum of this absorption band. After an energy calibration owing to Coulomb effects,[25,26] a mean diameter and a diameter distribution of 1.36 ± 0.25 nm is achieved (see Table 1) for the *sem*-SWNTs in our sample. The second interband transition of *sem*-SWNTs (Figure 2b) demonstrates three distinct maxima at 940, 1014, and 1082 nm, indicating that *sem*-SWNTs with diameters of 1.26, 1.37, and 1.48 nm dominate in the sample.

TABLE 1: Spectral Data and Assignment of the Interband Transions and Chiral Indices of SWNTs

abs. wavelength (nm)	interband transitions[a]	Calcd dia (nm)	ω_{RBM} (cm^{-1})	Raman dia[b] (nm)	(m, n)
438.13	$^1S_{33}$	1.181	190.4	1.18	(*11*,*6*)
350.96	$^1S_{44}$	1.182			(*9*,*8*)
584.12	$^1M_{11}$	1.180			(***10,7***)
940.65	$^2S_{22}$	1.267	179.3	1.25	(*11*,*7*)
465.68	$^2S_{33}$	1.255			
374.14	$^2S_{44}$	1.260			
625.44	$^2M_{11}$	1.264			(***12,6***)
309.69	$^2M_{22}$	1.252			
489.61	$^3S_{33}$	1.319	172.7	1.30	(*12*,*7*)
397.27	$^3S_{44}$	1.338			(*13*,*6*)
644.30	$^3M_{11}$	1.302			(***11,8***)
330.85	$^3M_{22}$	1.337			
1805.9	$^4S_{11}$	1.369[c]	161.6	1.38	(*12*,*8*)
1014.4	$^4S_{22}$	1.367			(*11*,*9*)
675.41	$^4M_{11}$	1.365			(***10,10***)
343.08	$^4M_{22}$	1.387			
519.62	$^5S_{33}$	1.400	161.6	1.38	(*14*,*6*)
418.33	$^5S_{44}$	1.409			
699.35	$^5M_{11}$	1.413			(***13,7***)
350.96	$^5M_{22}$	1.418			
1081.8	$^6S_{22}$	1.458	146.7	1.53	(*14*,*7*)
552.53	$^6S_{33}$	1.487			
438.13	$^6S_{44}$	1.476			
316.35	$^6S_{55}$	1.492			
734.64	$^6M_{11}$	1.485			(***15,6***)
367.29	$^6M_{22}$	1.485			
584.12	$^7S_{33}$	1.574	146.7	1.53	(*12*,*11*)
465.68	$^7S_{44}$	1.568			(*16*,*6*)
330.85	$^7S_{55}$	1.560			
784.13	$^7M_{11}$	1.585			(***13,10***)
387.55	$^7M_{22}$	1.567			

[a] $^jS_{ii}$ or $^jM_{ii}$ denotes the vertical interband transition between the *i*th van Hove singularities in both the valence and the conduction bands of a *sem*- or *met*-SWNT with *j*th diameter. [b] $d_t = 223.75/\omega_{RBM}$. [c] A calibrated datum.

The mean diameter and diameter distribution obtained here are in good agreement with the typical values measured by Raman scattering and TEM for the electric-arc-produced SWNTs with Y−Ni as catalyst.[27] Comparing with ref 22 and 23, both the first and the second optical absorption bands originating from *sem*-SWNTs shift to the higher-energy side. Reich et al. reported that bundling of the tubes to ropes results in a decrease of the energy gap in *sem*-nanotubes.[28] Thus, we argue that soluble SWNTs of high purity are well dispersed in our sample, which further confirms the validity of our dispersion/centrifugation cycles in dispersing and purifying SWNTs.

Observed in Figure 2c,d,e are fine structures, originating from the first and second interband transitions of *met*-SWNTs and the third, fourth, and fifth counterparts of *sem*-SWNTs. Analysis of them in details leads us to determine the diameter and chirality distributions, and hence the chiral indices (n, m) of SWNTs presented in our soluble sample.

Application of the above equation to the fine structures in Figure 2 yields discrete diameters for the SWNTs presented in the soluble sample. As shown in Table 1, all the features identified in Figure 2 (except the shoulders around 1180 and 2000 nm owing to the absorbed water in THF) are ascribed to the optical transitions of *met*- or *sem*-SWNTs with seven discrete diameters. Therefore, we identify all optically permitted transitions of the CarboLex SWNTs from the ultraviolet to the near-infrared side, and correlate them with *met*- and *sem*-SWNTs of seven discrete diameters. The existence of a structural gap in tube diameter between 1.26 and 1.32 nm predicted theoretically[29] and the speculation that *met*- and *sem*-SWNTs are synthesized with a similar diameter distribution are also confirmed by the quite good agreement in deduced diameters within each group.

Kuzmany et al. reported the mean diameters and diameter distributions of six nanotube samples achieved by a detailed analysis of the radial breathing mode (RBM) Raman response, optical spectra, and X-ray diffraction patterns.[30] It is of interest to note that five of the seven discrete diameters identified in Table 1 are in very good agreement with five mean diameters of their samples. Moreover, the fine structure in our optical absorption spectra (see Figure 1) could be reproduced with respect to the line position, width, and intensity by their fitting when an approximation is applied to the full set of DOS (the density of states) functions. They ascribed the origin of the fine structure in the optical response to a clustering of geometrically allowed diameters of the tubes, but they did not give the detailed discrete data.

We also checked out the diameter distribution in our soluble SWNTs by Raman scattering measurements. From Figure 3, the Raman spectrum of Solution 6 after evaporation of solvent, five maxima were identified. The observed RBM frequencies (ω_{RBM}) and calculated SWNTs diameters are also listed in Table 1. It can be seen that the deduced tube diameters both from optical absorptions and from the RBM frequencies are consistent with each other. Moreover, the distribution in intensity of the first and second semiconducting optical transitions and Raman scattering RBM frequencies agrees quite well upon the largest abundance of SWNTs with a diameter near 1.36 nm. Additionally, higher energy resolution of optical absorption than Raman scattering in distinguishing tube diameters is also evidenced in Table 1. Thus, the assignment on the fine optical structures made in Table 1 is supported by Raman scattering measurements.

Chattopadhyay et al.[21] reported a direct observation of "all optically allowed transitions" for both *met*- and *sem*-SWNTs, and assigned the features in UV−vis−NIR spectrum to the interband transitions of SWNTs with three discrete diameters

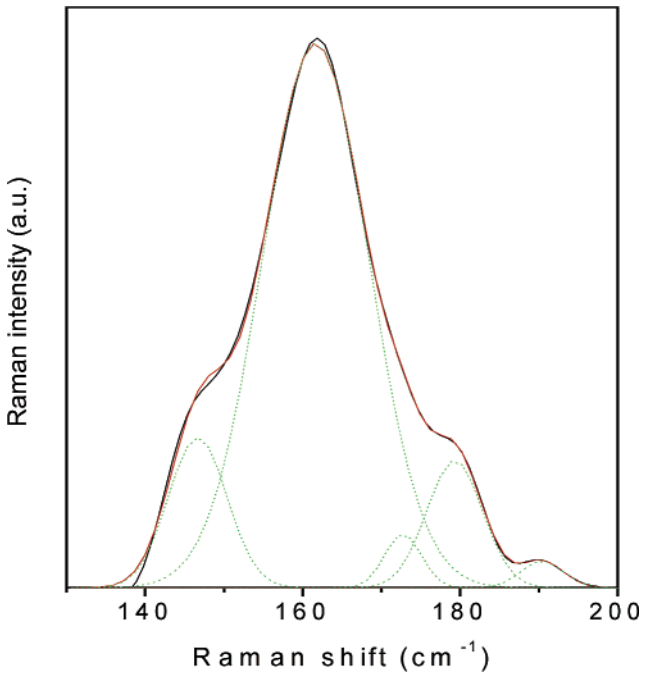

Figure 3. Gauss fitting (the green dot and red lines) of RBM in the Raman spectrum (the black lines) of Solution 6 (after evaporation of THF and excited with 514.5 nm laser).

of 1.22, 1.33, and 1.60 nm, respectively. Our spectral investigation on soluble SWNTs reveals some ambiguities in their work. First, according to the electronic band theory, "all optically allowed transitions" should include the first and second metallic and the third, fourth, and even fifth semiconducting band transitions for SWNTs with a mean diameter of ∼1.30 nm in the UV−vis spectrum. However, none of the fourth and fifth interband transitions for *sem*-SWNTs was assigned. Second, it is well-known that the laser-ablation produced SWNTs have a Gaussian function distribution in abundance centered at 1.2 or 1.4 nm diameter, and the yield of 1.6 nm SWNTs is very low.[31] Therefore, it is also doubtful for the assignment of 1.60 nm diameter SWNTs in their work.

Furthermore, optical absorption spectroscopy can also give information on distribution in nanotube chirality. Previous works[4,32] prove that tube chirality has a strong effect on optical absorption. Details of the second interband transition of *sem*-SWNTs (Figure 2b) and the first one of *met*-SWNTs (Figure 2c) including the number and relative intensity of subpeaks or shoulders agree very well with the tight-binding-based fitting[4] and the calculated optical absorption functions with chiral angle (θ) confined to $15° \leq \theta \leq 30°$.[33] Furthermore, preferential formation of SWNTs with chirality close to armchair direction is concluded,[3,32] and chemical etching leads to a shift in chirality from the zigzag toward the armchair direction.[34] Thus, it is reasonable for us to ascribe the SWNTs in our sample of chirality close to the armchair axis. The diameter gap (Δd_t) ($0.04 \leq \Delta d_t \leq 0.08$ nm) for the seven discrete SWNTs assigned in this work also provides additional support to such an assumption in tube chirality distribution.[3]

With the distributions in diameter and chiral angle outlined above, we can assign the (n, m) nanotube indices with diameter deviation of $-0.02 < \Delta d_t < 0.02$ nm and chiral angle distribution within $15° \leq \theta \leq 30°$, respectively. A SWNT is considered metallic if the value $n - m$ is divisible by 3. Otherwise, the nanotube is semiconducting. As shown in Table 1, seven (n, m) indices are assigned to *met*-SWNTs and eleven to *sem*-SWNTs. The accuracy of such assignment is largely

dependent on the resolvability of optical subpeaks or shoulders. Much better resolution in the first optical transition bands of *met*-SWNTs makes us sure that *met*-SWNTs are assigned more accurately than *sem*-SWNTs in this work.

Saito et al. discussed the chirality's dependence of the splitting in the VHS peaks for nanotube rope samples.[35] They concluded that such splitting is only important for thin metallic nanotubes with small chiral angle, and no splitting is obtained for armchair or semiconducting nanotubes. The SWNTs present in our sample are identified as of chirality close to the armchair axis, and the arc-produced tubes could not be ascribed as "thin" in comparison with the laser-produced or HiPCO species. It should be mentioned that our optical measurements are made in the solution phase, in which SWNTs are separated individually or in very small bundles, so that the interactions among SWNTs are significantly minimized. Moreover, the average energy position of the VHS peaks depends only on the nanotube diameter, and only those symmetric transitions between singularities from the valence band to those in the conduction band are optically allowed. Therefore, the width of the peak splitting caused by the "trigonal warping effect" ought to be limited in a small scale, and determination of the locations of the singularities from optical spectra would lead to an acceptable accuracy. Nonetheless, the somewhat nonlinear correlation between the energy of singularities noted by Saito et al. ought to be taken into account in the detailed interpretation of the optical transmission data. Unfortunately, up to the present there is no sophisticated method available to make such a correction.

Here, we demonstrate a convenient approach to assign the chiral indices (n, m) of SWNTs well dispersed in solution. Solution phase optical spectroscopy has its advantage over STM/STS and Raman scattering when applied to determine the electronic and atomic structures of SWNTs. Both STM/STS and Raman scattering are usually carried out on some kind of substrate with SWNTs sprayed on it. Thus, the interaction among SWNTs and that between tubes and substrate have to be accounted for. Because of the limited number of SWNTs studied, it is hard to get reliable statistics with STM/STS. In addition, it is also a technical challenge to operate the STM/STS system. Though resonant Raman spectroscopy can be used to determine the diameter distribution of SWNTs, it can provide less information on tube chirality. Furthermore, a good resonant condition for carbon nanotubes is not easy to obtain using a given laser energy.

As a matter of fact, our success in assigning the SWNTs presented in our soluble samples lies in the availability of high-energy resolution in the optical absorption spectra. We argue that the purity and aggregating state of SWNTs (individual or bundling) in a sample play an important role in the optical fine structure. To date, three commercially available SWNTs, i.e., CarboLex (1.34 nm, electric arc), tubes @Rice (1.21 nm, laser oven), and HiPco (0.81 nm, HiPco 10 atm material) are widely investigated. Fine structure in optical absorption spectra is usually observed for HiPco and Tubes @Rice SWNTs whether in solid thin films or in the suspension phase.[3,10] In contrast, only a few optical bands are observed so far for CarboLex SWNTs. This reflects their differences both in purity and in tube diameter. The higher tube abundance in HiPco and Tubes @Rice products than that of CarboLex is the main factor leading to their higher resolvability in optical spectra. On the other hand, because of the inversely proportional relationship between the nanotube diameter and the energy of the absorption features, $\Delta E \sim 1/d_t$, the larger mean tube diameter (~1.4 nm) of CarboLex SWNTs is also expected to be responsible for the lower resolution of their optical absorption spectra.

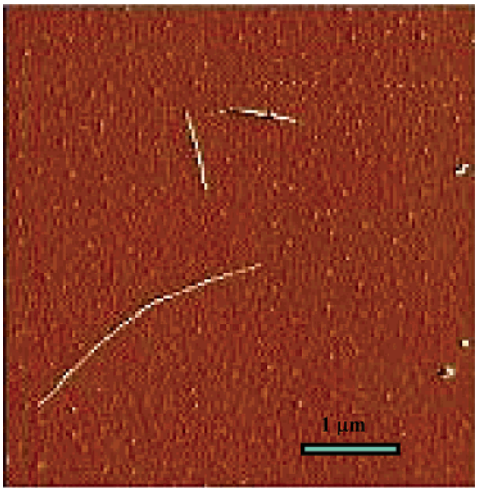

Figure 4. A typical AFM image of Solution 6 on a freshly cleaved mica surface observed in the tapping-mode of operation.

Typically, the raw CarboLex SWNTs contains catalyst metal particles, metal clusters encapsulated in graphite layers, amorphous carbon, and in some cases fullerenes, with a 30-wt % abundance of carbon nanotube ropes. In our wet chemical process, most of the SWNTs ropes are unbundled and well dispersed in THF solution. Large tube bundles, aggregates of nonnanotube carbon structures, and residual catalyst are removed as sediment by repeating dispersion/centrifugation. Fine functionalized amorphous carbon and metal clusters encapsulated in graphite layers are more soluble than functionalized SWNTs, and most of them are fractionated into the samples before Solution 6. The UV−vis−NIR spectra of Solutions 1 to 10 (Figure 1) support such an assumption. The blue shift in the first and second transitions of *sem*-SWNTs (Figure 2a,b) compared with previous works confirms that high-quality SWNTs are well dissolved in Solution 6. On the other hand, aggregation of nanotubes into bundles and coexistence with impurities in SWNTs sample will substantially broaden the absorption features. We interpret such band broadening to be due to the van der Waals interaction among SWNTs in bundles and that between individual tubes and impurities. In this sense, optical absorption spectroscopy also offers a convenient and effective assay to evaluate the purity as well as the aggregating state of SWNTs.

Further support for the purity as well as dispersibility of our functionalized nanotubes comes from AFM measurement. Shown in Figure 4 is a typical AFM image of Solution 6, in which well-separated SWNTs with clean surfaces are observed, whereas very few fine carbon particles are detected. Normally, the length of the soluble SWNTs is around 1 μm. A small tube bundle as long as 3 μm is shown in Figure 4. In comparison with ref 21, many longer SWNTs have survived in the mixed acids etching process. We suppose that the coated amorphous carbons prevent the $K_2S_2O_8$-oxidized SWNTs from severe etching and generating SWNTs debris.[36]

Recently, photoluminescence of HiPco SWNTs and MWNTs was reported to be of similar structure to their absorptions,[10,37] which confirms the VHSs in the density of states of carbon nanotubes. Despite the differences in purity and atomic structures among CarboLex, HiPco SWNTs, and MWNTs, these results provide additional support to the assignment of the absorption data presented in this work.

4. Conclusions

In summary, a wet chemistry procedure was successfully applied to prepare well-separated SWNTs of high quality, which makes it possible to resolve the fine optical structure originating from interband electronic transitions for a number of *met*- and *sem*-SWNTs. Detailed analysis of the optical data reveals that CarboLex SWNTs are formed with preferred distributions in diameters and chiral angles. Moreover, a chiral indices (*n*, *m*) assignment was also made for those SWNTs well dispersed in solution phase. Further study on the continuous dispersion−centrifugation cycles may lead to separation of metallic and semiconducting nanotubes.

Acknowledgment. This study was partly supported by the Industrial Technology Research Grant Program '02 from New Energy and Industrial Technology Development Organization (NEDO) of Japan, and a Grant-in-Aid and the 21st Century COE Program from the Ministry of Education, Culture, Sports, Science and Technology.

References and Notes

(1) Kataura, H.; Kumazawa, Y.; Maniwa, Y.; Umezu, I.; Suzuki, S.; Ohtsuka, Y. Achiba, Y. *Synth. Met.* **1999**, *103*, 2555.

(2) Hamada, N.; Sawada, S. I.; Oshiyama, A. *Phys. Rev. Lett.* **1992**, *68*, 1579.

(3) Jost, O.; Gorbunov, A. A.; Pompe, W.; Pichler, T.; Friedlein, R.; Knupfer, M.; Reibold, M.; Bauer, H. D.; Dunsch, L.; Golden, M. S.; Fink, J. *Appl. Phys. Lett.* **1999**, *75*, 2217.

(4) Liu, X.; Pichler, T.; Knupfer, M.; Golden, M. S.; Fink, J.; Kataura, H.; Achiba, Y. *Phys. Rev. B* **2002**, *66*, 045411.

(5) Chen, J.; Hamon, M. A.; Hu, H.; Chen, Y.; Rao, A. M.; Eklund, P. C.; Haddon, R. C. *Science* **1998**, *282*, 95.

(6) Kazaoui, S.; Minami, N.; Jacquemin, R.; Kataura, H.; Achiba, Y. *Phys. Rev. B* **1999**, *60*, 13339.

(7) Kazaoui, S.; Minami, N.; Matsuda, N.; Kataura, H.; Achiba, Y. *Appl. Phys. Lett.* **2001**, *78*, 3433.

(8) Jorio, A.; Saito, R.; Hafner, J. H.; Lieber, C. M.; Hunter, M.; McClure, T.; Dresselhaus, G.; Dresselhaus, M. S. *Phys. Rev. Lett.* **2001**, *86*, 1118.

(9) Wildöer, J. W. G.; Venema, L. C.; Rinzler, A. G.; Smalley, R. E.; Dekker, C. *Nature* **1998**, *391*, 59.

(10) O'Connell, M. J.; Bachilo, S. M.; Huffman, C. B.; Moor, V. C.; Strano, M. S.; Haroz, E. H.; Rialon, K. L.; Boul, P. J.; Noon, W, H.; Kittrell, C.; Ma, J.; Hauge, R. H.; Weisman, R. B.; Smalley, R. E. *Science* **2002**, *297*, 593.

(11) Chiang, I. W.; Brinson, B. E.; Smalley, R. E.; Margrave, J. L.; Hauge, R. H. *J. Phys. Chem. B* **2001**, *105*, 1157.

(12) Bahr, J. L.; Yang, J.; Kosynkin, D. V.; Bronikowski, M. J.; Smalley, R. E.; Tour, J. M. *J. Am. Chem. Soc.* **2001**, *123*, 6536.

(13) Baughman, R. H.; Zakhidov, A. A.; de Heer, W. A. *Science* **2002**, *297*, 787.

(14) Bandow, S.; Rao, A. M.; Williams, K. A.; Thess, A.; Smalley, R. E.; Eklund, P. C. *J. Phys. Chem. B* **1997**, *101*, 8839.

(15) Dalton, A. B.; Stephan, C.; Coleman, J. N.; McCarthy, B.; Ajayan, P. M.; Lefrant, S.; Bernier, P.; Blau, W. J.; Byrne H. J. *J. Phys. Chem. B* **2000**, *104*, 10012.

(16) Georgakilas, V.; Voulgaris, D.; Vazquez, E.; Prato, M.; Guldi, D. M.; Kukovecz, A.; Kuzmany, H. *J. Am. Chem. Soc.* **2002**, *124*, 14318.

(17) Chattopadhyay, D.; Galeska, I.; Papadimitrakopoulos, F. *J. Am. Chem. Soc.* **2003**, *125*, 3370.

(18) Yang, Y. L.; Zhang, J.; Nan, X. L.; Liu, Z. F. *J. Phys. Chem. B* **2002**, *106*, 4139.

(19) Liu, J.; Rinzler, A. G.; Dai, H. J.; Hafner, J. H.; Bradley, R. K.; Boul, P. J.; Lu, A.; Iverson, T.; Shelimov, K.; Huffman, C. B.; Rodriguez-Macias, F.; Shon, Y. S.; Lee, T. R.; Colbert, D. T.; Smalley, R. E. *Science* **1998**, *280*, 1253.

(20) Liu, Z. F.; Shen, Z. Y.; Zhu, T.; Hou, S. F.; Ying, L. Z.; Shi, Z. J.; Gu, Z. N. *Langmuir* **2000**, *16*, 3569.

(21) Chattopadhyay, D.; Lastella, S.; Kim, S.; Papadimitrakopoulos, F. *J. Am. Chem. Soc.* **2002**, *124*, 728.

(22) Zhao, B.; Hu, H.; Niyogi, S.; Itkis, M. E.; Hamon, M. A.; Bhowmik, P.; Meier, M. S.; Haddon, R. C. *J. Am. Chem. Soc.* **2001**, *123*, 11673.

(23) Chen, J.; Rao, A. M.; Lyuksyutov, S.; Itkis, M. E.; Hamon, M. A.; Hu, H.; Cohn, R. W.; Eklund, P. E.; Colbert, D. T.; Smalley, R. E.; Haddon. R. C. *J. Phys. Chem B* **2001**, *105*, 2525.

(24) Charlier, J. C.; Lambin, Ph. *Phys. Rev. B* **1998**, *57*, R15 037.

(25) Ichida, M.; Mizuno, S.; Saito, Y.; Kataura, H.; Achiba, Y.; Nakamura, A. *Phys. Rev. B* **2002**, *65*, 241407.

(26) Pichler, T.; Knupfer, M.; Golden, M. S.; Fink, J.; Rinzler, A.; Smalley, R. E. *Phys. Rev. Lett.* **1998**, *80*, 4729.

(27) Shi, Z.; Lian, Y.; Zhou, X.; Gu, Z.; Zhang, Y.; Iijima, S.; Li, H.; Yue, K. T.; Zhang, S. L. *J. Phys. Chem. B* **1999**, *103*, 8698.

(28) Reich, S.; Thomsen, C.; Ordejón, P. *Phys. Rev. B* **2002**, *65*, 155411.

(29) http://www.photon.t.u-tokyo.ac.jp/~maruyama/kataura/kataura.html.

(30) Kuzmany, H.; Plank, W.; Hulman, M.; Kramberger, Ch.; Grüneis, A.; Pichler, Th.; Peterlik, H.; Kataura, H.; Achiba, Y. *Eur. Phys. J. B* **2001**, *22*, 307.

(31) Rinzler, A. G.; Liu, J.; Dai, H.; Nikolaev, P.; Huffman, C. B.; Rodriguez-Macias, F. J.; Boul, P. J.; Lu, A. H.; Heymann, D.; Colbert, D. T.; Lee, R. S.; Fischer, J. E.; Rao, A. M.; Eklund, P. C.; Smalley, R. E. *Appl. Phys. A* **1998**, *67*, 29.

(32) Bachilo, S. M.; Strano, M. S.; Kittrell, C.; Hauge, R. H.; Smalley, R. E.; Weisman, R. B. *Science* **2002**, *298*, 2361.

(33) Lin, M. F. *Phys. Rev. B* **2000**, *62*, 13153.

(34) Odom, T. W.; Huang, J.; Kim, P.; Lieber, M. *J. Phys. Chem. B* **2000**, *104*, 2794.

(35) Saito, R.; Dresselhaus, D.; Dresselhaus, M. S. *Phys. Rev. B* **2000**, *61*, 2981.

(36) Zhao, B.; Hu, H.; Niyogi, S.; Itkis, M. E.; Hamon, M. A.; Bhowmik, P.; Meier, M. S.; Haddon, R. C. *J. Am. Chem. Soc.* **2001**, *123*, 11673.

(37) Brennan, M. E.; Coleman, J. N.; Drury, A.; Lahr, B.; Kobayashi, T.; Blau, W. J. *Opt. Lett.* **2003**, *28*, 266.